THE JOURNAL OF PHYSICAL CHEMISTRY C

Article

pubs.acs.org/JPCC

Reorientational Hydrogen Dynamics in Complex Hydrides with Enhanced Li^+ Conduction

Tatsiana Burankova,[†] Léo Duchêne,[‡,§] Zbigniew Łodziana,[⊥] Bernhard Frick,[∥] Yigang Yan,[#,‡] Ruben-Simon Kühnel,[‡] Hans Hagemann,[§] Arndt Remhof,[*,‡] and Jan P. Embs[*,†]

[†]Laboratory for Neutron Scattering and Imaging, Paul Scherrer Institute, 5232 Villigen PSI, Switzerland

[‡]Empa, Swiss Federal Laboratories for Materials Science and Technology, 8600 Dübendorf, Switzerland

[§]Département de Chimie-Physique, Université de Genève, 1211 Geneva, Switzerland

[⊥]INP, Polish Academy of Sciences, 31-342 Kraków, Poland

[∥]Institut Laue−Langevin, 38042 Grenoble, France

[#]Center for Materials Crystallography (CMC) and Interdisciplinary Nanoscience Center (iNANO), Aarhus University, 8000 Aarhus C, Denmark

Supporting Information

ABSTRACT: Lithium amide−borohydrides $Li[BH_4]_{1-x}[NH_2]_x$ possess liquid-like Li superionic conductivity at nearly ambient temperature. The fast Li^+ diffusion facilitated by the localized motions of the anions is proposed to occur through a network of vacant tetrahedral sites, acting as conduction channels. To study the reorientational dynamics of the anions, we have performed quasielastic neutron scattering experiments on samples with different compositions (x = 2/3, 0.722, 0.737, 3/4) over a broad temperature and time range. To unambiguously disentangle the contributions of the two species, $[BH_4]^-$ and $[NH_2]^-$, we took advantage of deuterium labeling and could clearly demonstrate that the quasielastic broadening is mainly determined by the $[BH_4]^-$ reorientations. With the help of a newly developed model, supported by *ab initio* molecular dynamics calculations, we have identified three relaxation components, which account for generally anisotropic C_3-rotations of the $[BH_4]^-$ tetrahedra including jumps by a small angle from the equilibrium position.

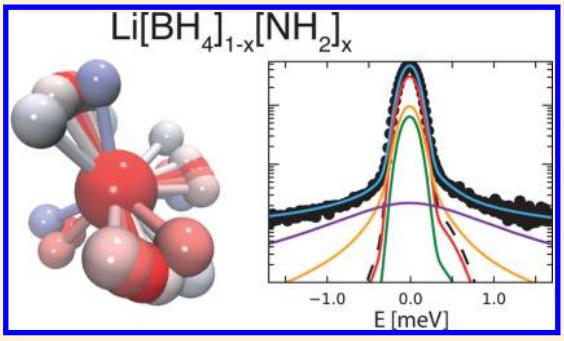

INTRODUCTION

Lithium complex hydrides with $[BH_4]^-$ and $[NH_2]^-$ anions have been mainly associated with hydrogen storage technologies due to their characteristically high volumetric and gravimetric hydrogen capacity.[1−4] Apart from this, recent research efforts have focused on another energy-storage related function of lithium amide-borohydrides, namely fast Li^+ ionic conduction.[5,6] Conductivities of 10^{-4}−10^{-3} S/cm at room temperature classify these materials as promising solid state electrolytes (SSE) for all-solid-state rechargeable batteries.[7] The best achieved conductivity of 6.4 × 10^{-3} S/cm (at 313 K) in an $[BH_4]^-$-rich lithium amide-borohydride[8] is comparable to typical values of liquid organic electrolytes used in lithium-ion batteries nowadays and, hence, these materials are competitive with the best SSE known to date.[9−12] The high conductivity in the understoichiometric $Li[BH_4]_{1-x}[NH_2]_x$ (2/3 < x < 3/4) has been attributed to the presence of a $[BH_4]^-$-rich side phase, coexisting with the stoichiometric x = 3/4 phase, commonly referred to as the α-phase in the $LiBH_4$−$LiNH_2$ pseudobinary phase diagram.[8] Lithium amide-borohydrides are characterized by lightweight, negligible electronic conduction, low grain boundary resistance, high thermal stability. Finally, the natural abundance of the constituent elements of these compounds is also considered advantageous in the development of new SSE.[7]

Composition dependent structures of $Li[BH_4]_{1-x}[NH_2]_x$ have been extensively studied by X-ray and neutron diffraction.[2,13−16] The $[BH_4]^-$ and $[NH_2]^-$ anions with nearly ideal geometry[15] form $\{Li[BH_4]_n^-[NH_2]_{4-n}^-\}$ tetrahedra with a Li-ion in the center. To ensure charge neutrality, there is another set of tetrahedra that remain empty and facilitate Li-migration.[8] The conductivities of the lithium amide-borohydrides are four or 5 orders of magnitude higher than that of the constituent materials, $LiBH_4$ and $LiNH_2$, at room temperature.[5,6] A comparable value of Li-conductivity in $LiBH_4$ can only be obtained above the temperature of the first-order phase transition from the low-temperature (LT) orthorhombic phase to the high-temperature (HT) hexagonal phase at 381 K.[17,18] These structural changes are accompanied not only by improved Li translational mobility, but also by significantly more rapid reorientational motion of $[BH_4]^-$ anions.[19,20] High anion jump rates have likewise been observed in the related systems, where the disordered HT-like phase is

Received: June 9, 2017
Revised: July 18, 2017
Published: July 24, 2017

DOI: 10.1021/acs.jpcc.7b05651
J. Phys. Chem. C 2017, 121, 17693−17702

stabilized by addition of lithium halides[21−23] or nanoconfinement[24,25] to improve the performance of the materials as SSE or for hydrogen-storage applications. In the case of larger anions, such as sulfates or phosphates, anion assisted ionic conduction has been discussed within the so-called "paddle-wheel" mechanism.[26,27] The model implies that rotational motion of polyatomic anions enhances the mobility of cations. Although the universal applicability of this idea is under discussion, the model points out that the mechanism of cation diffusion is more complicated than just conventional hopping and that the contribution from reorientations and center-of-mass fluctuations of the anions may be not negligible. Thus, acquiring sufficient knowledge about the relation between the crystal structure, anion reorientational dynamics and cation mobility holds the key for further improvement of ion-conducting and hydrogen-storage characteristics of these materials.

Since the microscopic dynamical description in mixed amide-borohydrides is scarce,[28] the goal of the present work was to investigate the reorientational motion of $[BH_4]^-$ and $[NH_2]^-$ units in $Li[BH_4]_{1-x}[NH_2]_x$ by means of quasielastic neutron scattering (QENS).[29] This technique has been successfully used to study dynamical properties of metal borohydrides and related compounds in the past decade.[19−21,30−33] Being sensitive to hydrogen, QENS also probes the relaxation time scale suited to resolve anion jump reorientations. Moreover, QENS delivers information on both spatial and time characteristics of studied processes. This is an advantage of the method compared with other valuable techniques such as solid-state nuclear magnetic resonance spectroscopy (NMR).[28,34,35] As both species, $[BH_4]^-$ and $[NH_2]^-$, contain hydrogen, the main challenge in the interpretation of QENS spectra would be to disentangle the two contributions. Nevertheless, the method provides a tool, namely deuterium labeling, to perform a sophisticated analysis. Thus, employing partially deuterated samples, we aimed to distinguish the $[BH_4]^-$ and $[NH_2]^-$ components, determine the geometry and evaluate the jump rates of anion motions. This detailed information about the microscopic dynamics is a requisite for understanding why mixed amide-borohydrides $Li[BH_4]_{1-x}[NH_2]_x$ have much better ion-conducting properties than the constituent materials.

EXPERIMENTAL SECTION

Samples. The lithium amide−borohydrides $Li[BH_4]_{1-x}[NH_2]_x$ (x = 2/3, 0.722, 0.737, 3/4) were synthesized and characterized as described previously.[8] To avoid the strong neutron absorption by the ^{10}B isotope in natural boron, ^{11}B-enriched $LiBH_4$ purchased from Katchem was used in the synthesis. $LiNH_2$ from Sigma-Aldrich and $LiND_2$ from Deutero were the precursors for the protiated and partially deuterated samples, respectively. The samples were handled in an Ar-filled glovebox to avoid air exposure.

IR characterization of the samples was performed on a temperature controlled Specac ATR setup mounted on a Biorad Excalibur FT-IR instrument in the frequency range between 600 and 4000 cm^{-1} with a resolution of 1 cm^{-1}.

Calculations. The experiments were complemented with sets of *ab initio* molecular dynamics (MD) calculations. The constant volume MD studies were performed with the Nose−Hoover thermostat,[36] and the time step 0.6 fs was chosen for integration of the equations of motions. For calculations of forces we used the Born−Oppenheimer approximation and the density functional theory (DFT). The core/valence electron interaction was described by the projector augmented wave method as implemented in the VASP package.[37,38] Atoms were represented by pseudopotentials with the valence electronic configurations $1s^22s^1$ for Li, $2s^22p^1$ for B, $2s^22p^3$ for N, and $1s^1$ for H. The exchange correlation functional was approximated by the Perdew−Burke−Ernzerhof generalized gradient approach,[39] and the wave functions were expanded in the plane wave basis set with the kinetic energy cutoff of 450 eV.

A single k-point was used for the MD calculations. All MD calculations were performed in a cubic unit cell with the experimental lattice constant 10.664 Å.[40] To approach dynamics of the system we used an enhanced temperature method and two independent sets of calculations were performed at 400 and 800 K. At each temperature the system was equilibrated for 5 ps followed by 15 ps of data collection. The stoichiometry of the system was changed by replacement of $[NH_2]^-$ by $[BH_4]^-$, keeping the volume of the unit cell constant.

To illustrate rotational mechanisms of different species, we calculated the projection of the vectors linking the central B or N atom with the hydrogen atoms of the corresponding anion $r(t) = \langle \vec{r}(t)\cdot\vec{r}(0)\rangle$, where the time lag t ranged from 1.2 fs to 5 ps, $\vec{r}(0)$ and $\vec{r}(t)$ are the unit vectors ($\overrightarrow{BH}/|\overrightarrow{BH}|$ or $\overrightarrow{NH}/|\overrightarrow{NH}|$) at the initial time point and at the time lag t, respectively. For each $[BH_4]^-$ there are four such autocorrelation functions, while two are necessary to describe rotational dynamics of $[NH_2]^-$.

Neutron Experiment. QENS measurements were performed on the cold neutron time-of-flight spectrometers FOCUS at Paul Scherrer Institute in Villigen, Switzerland[41,42] and IN16B at the Institut Laue−Langevin in Grenoble, France.[43] The instruments operate on significantly different time scales and, hence, we could follow the quasielastic signal in a broad temperature range from 150 to 425 K.

At IN16B[44] a neutron wavelength of λ = 6.271 Å was selected, which corresponded to the resolution of 0.8 μeV (full width at half-maximum, fwhm). The wavevector transfer available with this setting ranged from 0.2 to 1.9 $Å^{-1}$. Two types of measurements were performed on IN16B. First, both elastic and inelastic fixed window scans (EFWS and IFWS)[45] were recorded at a rate of 1.0−2.0 K/min. Second, we used the QENS mode with a Doppler drive changing the wavelength of incident neutrons to obtain spectra at several selected temperatures in the dynamical range of ±30 μeV. The samples with the thickness of 1 mm were measured in an aluminum flat sample holder positioned in transmission geometry at 135° to the incident beam. The necessity to use relatively "thick" samples is explained by the presence of natural Li, which also absorbs neutrons, although to a less extent than natural B.

The experiments on FOCUS were performed with a wavelength of incident neutrons of λ = 4.0 Å. The resolution of 0.220 meV (fwhm) and a much broader energy transfer window (∼2−3 meV) were needed to study anion reorientational dynamics at temperatures above 300 K. The spectra were binned in a range of scattering vectors of Q = 0.5−2.5 $Å^{-1}$. The sample containers used on FOCUS had a hollow cylindrical geometry with the gap width of 1 mm between the inner and outer cylinder and the outer diameter of 12 mm.

Additional runs with vanadium standards and empty sample containers were carried out on both spectrometers to perform typical corrections for experimental distortions. The procedure included vanadium normalization, detector efficiency correction and background subtraction. The sample attenuation and self-shielding factors were calculated with respect to the geometry of the experiment. The standard data reduction of the IN16B data

DOI: 10.1021/acs.jpcc.7b05651
J. Phys. Chem. C 2017, 121, 17693−17702

was performed using the LAMP[46] software package. The DAVE[47] package was used for both the data reduction of the FOCUS spectra and further examination of all the data sets at individual Q-groups.

The sample thickness of 1 mm unavoidably led to pronounced effects of multiple scattering, which could not be neglected in this case. To eliminate its influence, multiple scattering corrections were performed with the help of the McStas software (http://mcstas.org) in an iterative way. The input files with the scattering function were generated using the model function described in the following section on the doubled momentum-range as compared to the experimentally accessible one.

For both instruments, the QENS spectra were analyzed in a program module,[48] which performs two-dimensional surface fits. This approach enables obtaining more stable and consistent results, as simultaneous fits with both E and Q being independent variables reduce the total number of free parameters to be adjusted.

RESULTS AND DISCUSSION

Data Analysis. The analysis of stochastic motions in $Li[BH_4]_{1-x}[NH_2]_x$ is significantly simplified owing to the large incoherent cross section of hydrogen. Even for the partially deuterated samples the measured intensity, I_{meas}, is dominated by incoherently scattered neutrons. In this case, only single-particle dynamics have to be considered. Hence, the QENS analysis is based on the fitting of experimental data to a model incoherent dynamic structure factor, $S(Q,E)$, convoluted with the resolution function of the instrument, $R(Q,E)$:

$$I_{meas} \sim \exp(-2W)S(Q, E) \otimes R(Q, E) + bk(Q) \quad (1)$$

where $\exp(-2W)$ is the Debye−Waller factor and $bk(Q)$ is a flat background accounting for faster motions, which cannot be resolved on the available experimental time scale.

The reorientational motions of the $[NH_2]^-$ anions[49] have been studied less extensively than those of the $[BH_4]^-$ anions.[19,20,50,51] A low symmetry environment of the amide group would allow only 180°-flips around its 2-fold axis, whereas other jump rotations (90°-tumbling in the cubic phase, C_4-uniaxial rotation in the tetragonal phase) are possible around additional axes provided by the site symmetry.[49] The geometry of $[BH_4]^-$ reorientations is also defined by the distances within the crystal and its symmetry. In the LT orthorhombic phase of bulk $LiBH_4$ the dominating motion is a 3-fold jump rotation around the C_3 axis.[19,25,52] For the HT hexagonal phase the trigonal disoder model was proposed,[20,25] where the $[BH_4]^-$ unit undergoes rapid reorientational jumps, accompanied by quasi-free jumps of the three trigonal hydrogen atoms about the C_3 axis of the anion (parallel to the crystallographic c axis). However, none of these models were appropriate to consistently describe the reorientational dynamics of the $[BH_4]^-$ groups in $Li[BH_4]_{1-x}[NH_2]_x$ in a broad temperature range. Therefore, we propose a modification of the 120°-tumbling model[53] with a certain degree of anisotropy in the jump rates. The idea is illustrated in Figure 1. The C_3-axes are not equivalent and the jump rate around one of them, $1/\tau$, is different (faster) than around the other three, $1/\tau_0$. There are additional sites (α and β) at an angle θ from the equilibrium positions 1, 2, and 3. The radius of the circle, on which the H atoms are located, can be calculated from the B−H bond length, r_{B-H}, as $r_0 = \frac{2\sqrt{2}}{3} r_{B-H}$. Fast jumps with the residence time τ_f can be performed in the following directions: $n \rightarrow n_\alpha$, n_β, or $n_\alpha \rightarrow n$ and $n_\beta \rightarrow n$, $n \in \{1, 2, 3\}$. Thus, the sites are not equivalent, and the occupational probability of any n-th site is 1/8 and any n_α, n_β-th site is 1/16. This simplified picture served to mimic disorder around the equilibrium positions, which can be significant in mixed amide-borohydrides as has been shown in simulations.[54,55]

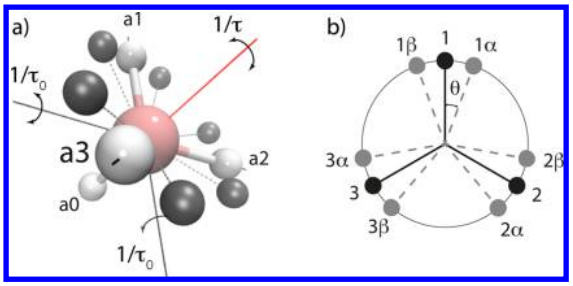

Figure 1. (a) Scheme of the jump model presented in eqs 2−5. The arrows indicate the reorientational motion about the C_3-axes denoted as a0, a1, a2, and a3. The jump rates equal $1/\tau$ around a0 and $1/\tau_0$ around the other three axes. (b) View along the a0-axis illustrating deviations from the equilibrium positions by an angle θ on the circumference of the circle.

The presented scheme of jump reorientations has common features with the models proposed by Verdal et al.[20] The advantage of our approach is that it is applicable for a broad temperature range, in which the character of reorientational dynamics gradually changes. Moreover, the focus of the earlier study[20] was mainly the fraction of elastically scattered neutrons, or elastic incoherent structure factor (EISF), whereas the complete analytical expression of the dynamic structure factor is required to profit from the simultaneous surface fits in the (Q,E)-domain employed in our analysis.

Following the classical methodology,[53,56,57] we solved the rate equations given in the Supporting Information (eq S1) and derived the dynamic structure factor $S_{rot120\_\theta}(Q,E)$ for the proposed model:

$$S_{rot120\_\theta}(Q, E) = \mathbb{L}(E)\mathbb{S}\mathbb{B}(Q) \quad (2)$$

where $\mathbb{L}(E)$ is the row-vector of Lorentzian functions $\mathcal{L}(\Gamma_i, E)$ with the following line widths:

$$\Gamma = \hbar\left[0,\ \frac{4}{\tau_0},\ \left(\frac{4}{\tau_0}+\frac{2}{\tau_f}\right),\ \left(\frac{4}{\tau_0}+\frac{1}{\tau_f}\right),\ \frac{1}{2}\left(\frac{5}{\tau_0}+\frac{3}{\tau}\right),\ \frac{1}{2}\left(\frac{5}{\tau_0}+\frac{3}{\tau}+\frac{4}{\tau_f}\right),\ \frac{1}{2}\left(\frac{5}{\tau_0}+\frac{3}{\tau}+\frac{2}{\tau_f}\right),\ \frac{2}{\tau_f},\ \frac{1}{\tau_f}\right] \quad (3)$$

$$\mathbb{S} = \frac{1}{128}\begin{bmatrix} 17 & 66 & 12 & 12 & 12 & 3 & 3 & 3 \\ 27 & -42 & 4 & 4 & 4 & 1 & 1 & 1 \\ 3 & 6 & -4 & -4 & -4 & 1 & 1 & 1 \\ 2 & 4 & 0 & 0 & 0 & -2 & -2 & -2 \\ 24 & -24 & 32 & -16 & -16 & 8 & -4 & -4 \\ 24 & -24 & -32 & 16 & 16 & 8 & -4 & -4 \\ 16 & -16 & 0 & 0 & 0 & -16 & 8 & 8 \\ 9 & 18 & -12 & -12 & -12 & 3 & 3 & 3 \\ 6 & 12 & 0 & 0 & 0 & -6 & -6 & -6 \end{bmatrix} \quad (4)$$

$\mathbb{B}(Q)$ is the column-vector of spherical Bessel functions of the zeroth order:

DOI: 10.1021/acs.jpcc.7b05651
J. Phys. Chem. C 2017, 121, 17693−17702

$$\mathbb{B}(Q) = \begin{bmatrix} 1 \\ j_0(Qr_0\sqrt{3}) \\ j_0\left(2Qr_0 \sin\frac{\theta}{2}\right) \\ j_0\left(2Qr_0 \sin\left(\frac{\pi}{3} - \frac{\theta}{2}\right)\right) \\ j_0\left(2Qr_0 \sin\left(\frac{\pi}{3} + \frac{\theta}{2}\right)\right) \\ j_0(2Qr_0 \sin\theta) \\ j_0\left(2Qr_0 \sin\left(\frac{\pi}{3} - \theta\right)\right) \\ j_0\left(2Qr_0 \sin\left(\frac{\pi}{3} + \theta\right)\right) \end{bmatrix} \quad (5)$$

In the limit $\theta \to 0$ at very low temperatures or if τ_f becomes too fast to be resolved on the time scale of the experiment, eqs 2−5 can be simplified, and the dynamic structure factor reads:

$$S_{rot\_120}(Q, E) = \frac{1}{4}(1 + 3j_0(Qr_0\sqrt{3}))\delta(E) + \frac{1}{4}(1 - j_0(Qr_0\sqrt{3}))\mathcal{L}(\Gamma_1, E) + \frac{1}{2}(1 - j_0(Qr_0\sqrt{3}))\mathcal{L}(\Gamma_2, E) \quad (6a)$$

$$\Gamma_1 = \frac{4\hbar}{\tau_0};\ \Gamma_2 = \frac{\hbar}{2}\left(\frac{3}{\tau} + \frac{5}{\tau_0}\right) \quad (6b)$$

The distance between two hydrogen atoms in the borohydride tetrahedra is $r_{H-H} = r_0\sqrt{3}$ and, if $\tau = \tau_0$, eq 6 transforms into the well-known 120°-tumbling model.[53] If $\tau_0 \gg \tau$, the scattering function corresponds to the uniaxial 3-jump rotation with one axial hydrogen being immobile. Thus, the derived eqs 2−5 include broadly applied models and provide the possibility to fit QENS spectra in the intermediate temperature range, when the mechanism of jump rotation gradually changes.

Both elastic and inelastic fixed window scans (EFWS and IFWS) can be analyzed in terms of the discussed models. In our experiment the EFWS and IFWS are proportional to the experimentally measured intensity in the channels $E_{off} = 0$ and 2 μeV, respectively. Taking into account that the dynamic structure factor of restricted jump motions can be written in a general way as

$$S(Q, E) = \exp(-2W(T))\{A_0(Q)\delta(E) + \sum_i A_i(Q)\mathcal{L}(\Gamma_i(T), E)\} \quad (7)$$

then, the temperature dependence of the fixed window scans is presented by the following equation:

$$I_{EFWS}(T),\ I_{IFWS}(T) \sim \exp(-2W(T))\{A_0(Q)R(E_{off}) + \sum_i A_i(Q)\tilde{R}(\sigma_{res}, \Gamma_i(T), E_{off})\} \quad (8)$$

where A_0 and A_i are the elastic and quasielastic incoherent structure factors, respectively, $R(E)$ is the experimental resolution function with the line width of σ_{res}, and $\tilde{R}(\sigma_{res}, \Gamma_i(T), E)$ is the convolution of the Lorentzian component, $\mathcal{L}(\Gamma_i(T), E)$, with the resolution function.

The last point to mention is that the QENS analysis does not permit to distinguish between the uniaxial C_2-reorientations with all four hydrogen atoms performing jumps and the uniaxial C_3-reorientations with one immobile atom on the axis of rotation discussed above. The same remains valid for the models taking into account jump motions with different rates. The dynamic structure factor for the prevailing C_2-mechanism has the same expression (eq S9 of the Supporting Information) from a formal mathematical point of view as eq 6. However, jump motions around the C_3 axis correspond better to the symmetry of the local environment of the $[BH_4]^-$ units in the cubic α-phase of $Li[BH_4]_{1/4}[NH_2]_{3/4}$.[15] This is further evidenced by IR spectra in the frequency range of the $[BH_4]^-$ bending modes (Figure S3 of the Supporting Information), which display characteristic changes upon a symmetry reduction from T_d for ideal $[BH_4]^-$ tetrahedra to C_{3v} because of a trigonal deformation.[58,59]

Our MD simulations also support the idea of the predominant C_3-reorientation mechanism for borohydride tetrahedra, which is illustrated with the angular autocorrelation functions in Figure 2.

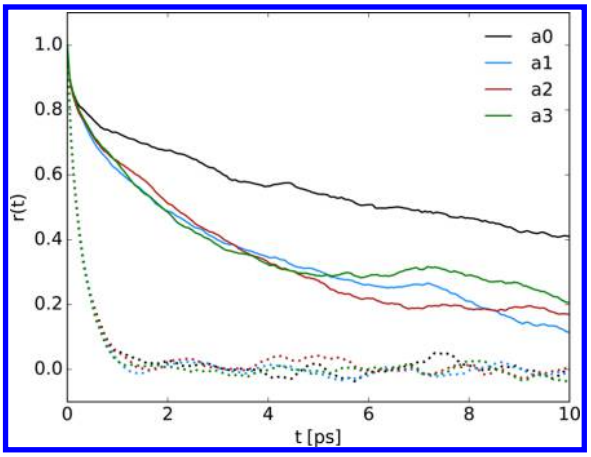

Figure 2. Autocorrelation functions of $[BH_4]^-$ determined from the MD simulations at $T = 400$ K (solid lines) and $T = 800$ K (dotted lines) for the $x = 0.656$ composition. The C_3 axes of rotation (a0, a1, a2, a3 in Figure 1) are assumed to be collinear to the B−H bonds at time 0.

If jump rotations occurred only around axis a0 (Figure 1), one component $r(t)$ would not change with time, which is valid in the low temperature regime within 15 ps of the simulation time. If reorientations around a1, a2, and a3 are also possible, but on a slower time scale, this component starts to decay. Indeed, as the temperature increases, jumps around various C_3 axes become more frequent. Owing to the difference in the relaxation times, it is still easy to distinguish $r(t)$ from the other three ones at $T = 400$ K. Any type of the C_2 model would not leave just one atom immobile or less mobile, and thus, can be ruled out. At higher temperatures the gap between the curves is smeared away, because rotations around all axes become equally probable. In contrast to the $[BH_4]^-$ tetrahedra, the $[NH_2]^-$ groups do not perform any reorientational motion at low temperatures (Figure S2 of the Supporting Information) within 15 ps of the simulation time, although this does not exclude a slower relaxation process. The amplitude of the $[NH_2]^-$ wiggling or librational dynamics is, nevertheless, large. Flips of the $[NH_2]^-$ units related to Li^+ translational motion start in the high temperature regime, where

DOI: 10.1021/acs.jpcc.7b05651
J. Phys. Chem. C 2017, 121, 17693−17702

the reorientational jump processes for both anions occur on the time scale of ~0.1 ps.

Anion Dynamics on Nanosecond and Picosecond Time Scale. The temperature dependence of the elastic intensity of $LiNH_2$ and $Li[BH_4]_{1-x}[NH_2]_x$ obtained on different time scales is displayed in Figure 3 and 4. In the picosecond time range

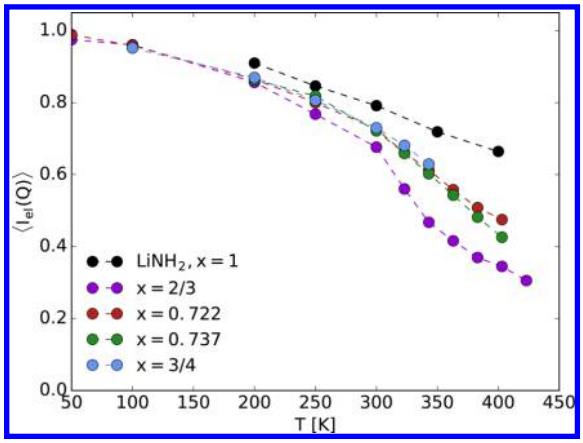

Figure 3. Elastic intensity of $LiNH_2$ and mixed lithium amide-borohydrides $Li[BH_4]_{1-x}[NH_2]_x$ measured on FOCUS and averaged over the analyzed Q-range as a function of temperature.

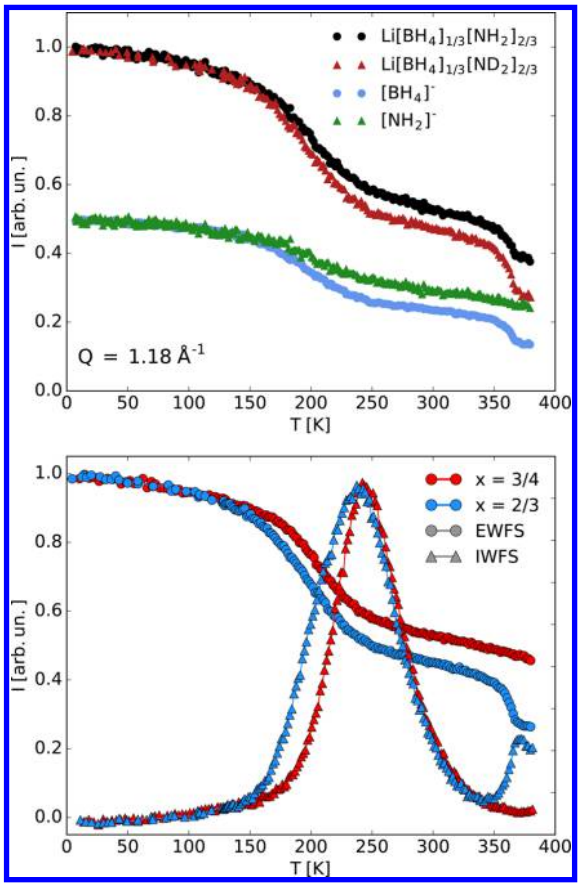

Figure 4. Upper panel: EFWS of the protiated and partially deuterated samples (x = 2/3) recorded on IN16B. The $[BH_4]^-$ and $[NH_2]^-$ contributions are the solutions of eq 9 and scaled to 0.5 at low temperature for clarity. Lower panel: EFWS (circles) and IFWS (triangles) of the partially deuterated samples $Li[BH_4]_{1-x}[ND_2]_x$ with x = 3/4 (red) and x = 2/3 (blue) averaged over the studied Q-range.

accessible on FOCUS the mixed samples show the onset of a quasielastic contribution above 300 K, whereas the gradual decrease of the elastic intensity in $LiNH_2$ is due to the temperature dependence of the Debye−Waller factor alone. From this observation we conjectured that the $[NH_2]^-$ groups probably do not contribute to the quasielastic broadening in the mixed compounds detected in the FOCUS experimental time window. The experiment on IN16B with protiated and partially deuterated samples provided an additional and convincing evidence of this idea (Figure 4).

Assuming that the samples scatter mainly incoherently and that $[BH_4]^-$ and $[NH_2]^-$ motions are not correlated, the dynamic structure factor of the protiated and deuterated sample can be expressed in the following way:

$$S_{prot}(Q, E) = \frac{4\sigma_H S_{BH4}(Q, E) + 2\left(\frac{x}{1-x}\right)\sigma_H S_{NH2}(Q, E)}{4\sigma_H + 2\left(\frac{x}{1-x}\right)\sigma_H} \quad (9a)$$

$$S_{deut}(Q, E) = \frac{4\sigma_H S_{BH4}(Q, E) + 2\left(\frac{x}{1-x}\right)\sigma_D S_{NH2}(Q, E)}{4\sigma_H + 2\left(\frac{x}{1-x}\right)\sigma_D} \quad (9b)$$

where $S_{BH4}(Q,E)$ and $S_{NH2}(Q,E)$ stand for the $[BH_4]^-$ and $[NH_2]^-$ contributions and σ_H and σ_D are the neutron incoherent scattering cross sections of hydrogen and deuterium, respectively. Equation 9 is basically a system of two linear equations, which can be solved in the whole scanned temperature range (Figure 4, upper panel). Apparently, all main characteristic step-like features on the nanosecond time scale in the mixed compounds originate from the $[BH_4]^-$ units. The decrease of the $[NH_2]^-$ elastic intensity is mostly due to vibrational and librational motions. These observations agree with the results of the DFT calculations, which show that the $[NH_2]^-$ groups only wiggle when the rotation of the $[BH_4]^-$ units sets in (Figure S2 of the Supporting Information).

The EFWS and IFWS of the samples with x = 2/3 and x = 3/4 are similar in the temperature range of 10−340 K (Figure 4, lower panel). The onset of the dynamics seen on FOCUS with a coarser resolution above 300 K is shifted to lower temperatures on IN16B, since intensity drop of EFWS or intensity increase of IFWS typical for thermally activated processes occur in the temperature range, where relaxation times, τ, fulfill the condition: $\hbar/\tau \sim \sigma_{res}$. These dynamics correspond to the rotational motion of the $[BH_4]^-$ groups and are similar to what was observed in the bulk $LiBH_4$.[30] The second characteristic decrease of the elastic intensity and the corresponding increase of the inelastic intensity can be seen only in the highly conducting sample with x = 2/3 above ~355 K, which can be related to a pronounced endothermic event at 313 K on heating.[8] The stoichiometric composition (x = 3/4) demonstrated a significantly smaller value of the latent heat at 313 K and this fact can account for the absence of the corresponding features in the EFWS and IFWS. The transition at 313 K is presumably associated with a side phase coexisting with the cubic α-phase for x = 2/3−3/4 and reported in literature,[8,13] the fraction of the side phase being larger in BH_4-rich samples. The presence of the side phase could also explain the temperature behavior of the IR spectra (Figure S3 of the Supporting Information), which demonstrate additional $[BH_4]^-$ bending modes that disappear upon heating. The structure of the dominating α-phase does not change above 313

DOI: 10.1021/acs.jpcc.7b05651
J. Phys. Chem. C 2017, 121, 17693−17702

K exhibiting only a slight thermal expansion. The trace of this transition can also be seen in the elastic intensity measured on FOCUS (Figure 3) for the $x = 2/3$ composition in the temperature range 300−350 K, where the steepness of the temperature dependence is larger than for the other samples.

Taking into account that only $[BH_4]^-$ rotational motions are resolved on the time scale of FOCUS and IN16B, the fraction of the hydrogen atoms in the borohydride anions, $p_{BH4} = 4/(4 + 2x/(1 - x))$, has to be added to the final expression of the dynamic structure factor:

$$S(Q, E) = (1 - p_{BH4})\delta(E) + p_{BH4}S_{model}(Q, E) \quad (10)$$

The FOCUS spectra at the highest available temperatures could be satisfactorily fitted with the simpler model describing C_3 jump reorientations (eqs 6 and 10). However, after having applied it for a broader temperature range, we found it inconsistent. It was clear that the underlying rotational mechanism was more complex. First, the relaxation times, τ_0 and τ, started decreasing for $T < 350$ K, which is unphysical. Second, it was necessary to accept that p_{BH4} might decrease with temperature as well. Third, we obtained an overestimated B−H bond length (>1.36 Å) in comparison to the literature values.[15,54]

The model independent analysis (eq 7) showed that the Q-dependence of the elastic incoherent structure factor (EISF, A_0 in eq 8) at low temperatures corresponds to a characteristic jump distance $\lesssim$1.0 Å, which is significantly less than the H−H distance in the $[BH_4]^-$ or $[NH_2]^-$ groups. Therefore, the model with additional jump sites was applied (Figure 1, eqs 3−5). In comparison with its predecessor, this function has two additional adjustable parameters, τ_f and θ, which is not generally favorable for the stability of fitting. Hence, we had to introduce some constraints. First, the B−H bond length was fixed to 1.225 Å as obtained from the analysis of the bulk $LiBH_4$ data with eq 6. This value is also in a good agreement with the previously published results[15,54,55] and the average bond length 1.228 Å from our MD calculations. Second, the fraction of rotating $[BH_4]^-$ units also remained restricted to the value determined from the nominal composition of a mixed compound. Finally, the parameters related to the fastest contribution were evaluated only for $T <$ 323 K. Their values in the high-temperature range were estimated by extrapolation and fixed as well.

The proposed model (Figure 1, eq 3−5) contains a sum of several Lorentzians, which can be grouped into the narrow ($\Gamma[2] = 4\hbar/\tau_0$, due to the 120°-reorientations around a1, a2, a3), medium ($\Gamma[5]=\hbar/2 \times (5/\tau_0 + 3/\tau)$, which contains the faster reorientational motion around a0) and broad quasielastic (all the other line widths) components. Their relative contributions to the total line broadening change with temperature, because all the three relaxation times are characterized by different activation energies. This statement is illustrated by Figure 5. At elevated temperatures the broadest component is almost identical to a flat contribution. This explains why the fits with the simpler model (eqs 6 and 10), in principle, work nicely. At low temperatures, the narrowest contribution becomes unresolved and is basically proportional to the resolution function; the broadest Lorentzian, on the contrary, appears to be distinguishable under these experimental conditions. The usage of eqs 6 and 10 in this temperature range leads to the erroneous temperature dependence of p_{BH4} and the relaxation times.

The relaxation time of fast oscillations, τ_f, is about 1 ps at $T =$ 250−323 K and does not depend on the composition of the mixed amide-borohydrides within the margin of error. The θ-value is about 15−17° at 250 K and increases with temperature,

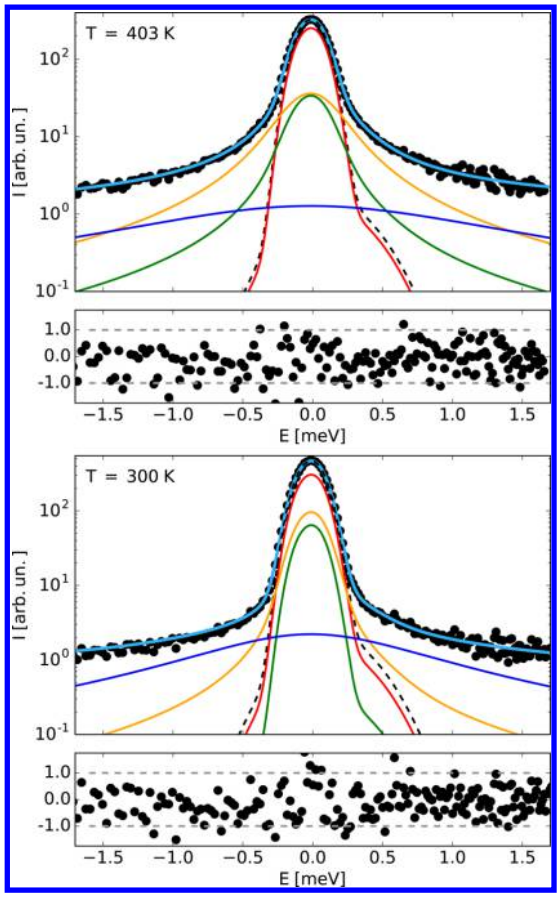

Figure 5. Experimental spectra of $Li[BH_4]_{1-x}[NH_2]_x$ ($x = 0.722$) at $Q =$ 2.4 Å^{-1}, fits to eqs 2−5 (120°-tumblings combined with deviation jumps) and residuals at selected temperatures. The lines in the plots are the resolution function (dashed black), total fit curve (light blue), pure elastic component (red), narrow (green), medium (orange), and broad (dark blue) components.

but as soon as the slowest component can be reliably resolved, θ has to be fixed together with τ_f. The estimate of the activation energy for the fastest component gives $E_A = 3.6 \pm 0.5$ kJ/mol. For the sake of mathematical simplicity, we considered deviations only around positions 1, 2, 3 (Figure 1). This definitely does not rule out a more complicated scheme of jump sites. Moreover, we still cannot completely exclude the possibility that this relaxation process partially originates from the $[NH_2]^-$ anions, which can oscillate with an amplitude of about 45° according to the MD simulations (Figure S2 of the Supporting Information). Since the quasielastic incoherent structure factors (QISF, A_i in eq 7) of the fastest contribution are much less than those of the other two components, it could appear in the IFWS (Figure 4, lower panel) only as a weak shoulder before the main bump. However, if it existed, the statistical quality of the data in this temperature range does not allow us to see any difference between the partially deuterated and protiated samples and, hence, to prove or disprove the $[NH_2]^-$ contribution. Broad quasielastic features were also described in several works on disordered systems and attributed to overdamped anion vibrations characterized by mean-squared displacement distances $\sqrt{\langle u^2 \rangle}$.[60,61] If the latter interpretation is accepted in the analysis of our data, then the intensity dependence of the fast component on Q[60] yields, for example, $\sqrt{\langle u^2 \rangle}$=0.33 Å at $T = 300$ K. At the same time, the jump distance between sites n, n_α or n, n_β equals 0.40 Å. This illustrates

DOI: 10.1021/acs.jpcc.7b05651
J. Phys. Chem. C 2017, 121, 17693−17702

that our model description with librational motions by an angle θ may be closely related to the concept of the overdamped vibrational modes.

Figure 6 displays the temperature dependencies of the $[BH_4]^-$ reorientational relaxation times in $Li[BH_4]_{1-x}[NH_2]_x$ calculated

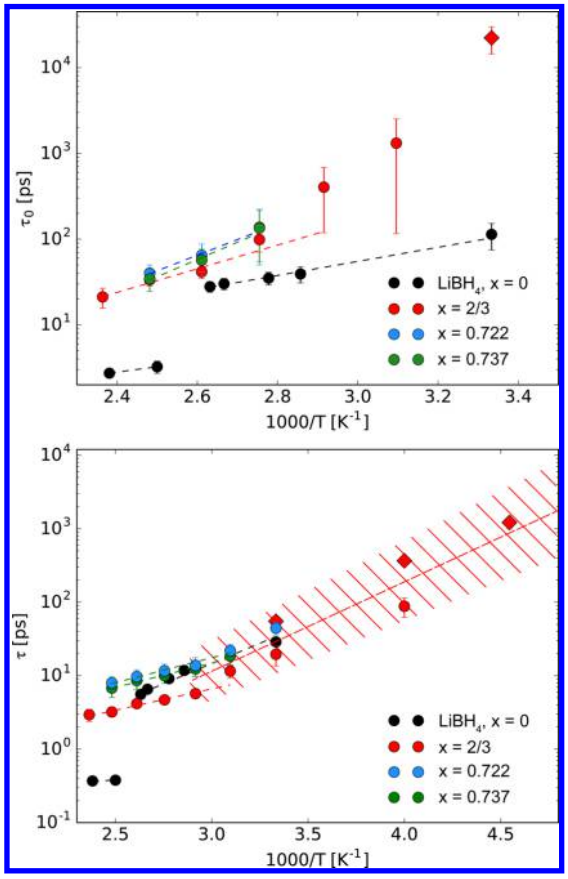

Figure 6. Temperature dependence of the relaxation times related to the slow reorientation of the whole $[BH_4]^-$ anion (τ_0, upper panel) and the fast uniaxial jumps around one C_3 axis (τ, lower panel). The FOCUS and IN16B results are plotted in circles and diamonds, respectively. The hatched area illustrates the range of the relaxation times described with a distribution of activation energies as obtained from the fits of the IFWS. The dashed lines are fits to the Arrhenius equation.

from the QENS spectra recorded on both instruments. For comparison, we also performed a reanalysis of the $LiBH_4$ data[19] in terms of eq 6. The more sophisticated surface fitting procedure allowed us to resolve the two relaxation times for the bulk $LiBH_4$ as well. The activation energies of these two components (Table 1) are in a good agreement with the result of the previously published study performed on IN16B[30] and close to the values reported in NMR and Raman spectroscopy studies.[34,62] The

Table 1. Best Fit Parameters of the Temperature Dependence of the Relaxation Times, τ_0 and τ, Obtained on FOCUS to the Arrhenius Equation (eq 11) in the Temperature Range T = 323−423 K

$Li[BH_4]_{1-x}[NH_2]_x$	$\tilde{\tau}_0$, fs	E_{A0}, kJ/mol	$\tilde{\tau}$, fs	E_A, kJ/mol
x = 0, low-T phase	190(80)	16(1)	7(3)	21(3)
x = 2/3	12(10)	26(7)	90(50)	12(2)
x = 0.722	1(1)	35(4)	160(70)	13(1)
x = 0.737	0.4(0.3)	38(6)	150(50)	13(1)

slowest process associated with the uniform rotation of the whole $[BH_4]^-$ anion is at the limit of the FOCUS resolution even at elevated temperatures. This explains large error bars in the middle of the available data range. Nevertheless, it is possible to notice that the activation energy increases on cooling the sample. A similar observation can be made in the case of the second component that accounts for the faster uniaxial C_3 motion. The two regions with a larger (T < 320 K) and smaller (T > 340 K) activation energies are even more pronounced. This temperature behavior correlates with that established for the Li-conductivity[8] and is a new example of coupling between Li-mobility and enhanced anion dynamics.

At first sight, the difference between the relaxation times measured on FOCUS and IN16B is significant (Figure 6) even allowing for resolution effects, because the analysis of the $LiBH_4$ data demonstrated that both instruments delivered consistent results. The answer can be found, if a broader temperature range available in the IWFS is analyzed. To fit the data to eq 8, we need to know the functional dependence of τ_0 and τ on temperature. Assuming that both relaxation times follow the Arrhenius law with the activation energy E_A and the pre-exponential factor $\tilde{\tau}$:

$$\tau = \tilde{\tau}\ \exp(E_A/RT) \tag{11}$$

we were not able to obtain physically reasonable values of the fit parameters. Indeed, the fits of the individual QENS spectra at T = 220, 250, and 300 K measured on IN16B showed that the origin of the quasielastic broadening at lower temperatures is mainly the uniaxial C_3-reorientation, the slowest component being too narrow even at T = 300 K. It affects the high-temperature wing of the IFWS curve, but does not have any influence at T < 300 K and, hence, cannot determine the broad shape of the IFWS curves. A single component with a smaller value of the activation energy, E_A, could extend the IFWS signal over a broader temperature range, however, the resulting line is highly asymmetrical.[45] Therefore, we included a Gaussian distribution of activation energies into our analysis, which is quite common for solid solutions with mixed anions:[28,35]

$$\overline{I_{IFWS}}(T) = \int I_{IFWS}(E, T)G(E; E_A, \Delta E_A)\ dE \tag{12}$$

where $G(E; E_A, \Delta E_A)$ is the Gaussian function with the maximum at $E = E_A$ and the variance ΔE_A. This approach leads to a much better agreement between the experimental data and the model IFWS curves (Figure 7).

The results of the fits with the Gaussian distribution function are summarized in Table 2. The sample with the BH_4:NH_2 ratio of 1:2 (x = 2/3) exhibits a broader range of the activation energies than the x = 3/4 composition. The corresponding relaxation times, τ, are displayed in Figure 6, lower panel as a hatched area, which covers the values evaluated from the QENS spectra recorded both on FOCUS and IN16B. The distribution of the activation energies explains, why the final fit results strongly depend on the instrumental resolution, which was not the case for the bulk $LiBH_4$. Different local environments of the BH_4 groups in the mixed compounds, especially with the BH_4-rich side phase, as well as additional jump sites on the circumference of the circle can cause a change in the energy barrier for rotation. It is necessary to mention that the presence of multiple scattering effects can influence the estimates significantly. Unfortunately, because IFWS/EFWS encompass a broad temperature range, the correction procedure converges slowly and is very time-consuming and challenging as compared

DOI: 10.1021/acs.jpcc.7b05651
J. Phys. Chem. C 2017, 121, 17693−17702

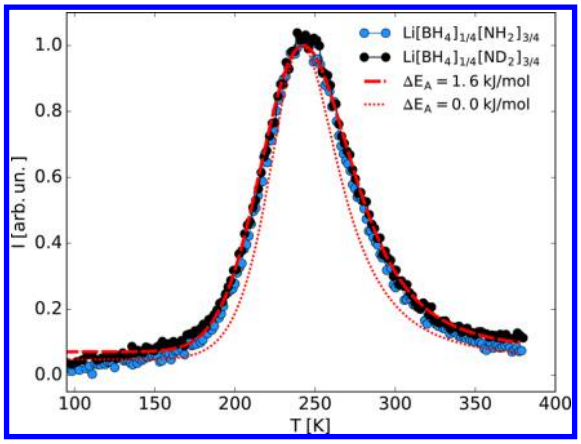

Figure 7. IFWS of the protiated (blue circles) and partially deuterated (black circles) samples with $x = 3/4$ at $Q = 1.18$ Å^{-1} recorded on IN16B. The red lines are the model IFWS curves taking into account the uniaxial C_3-reorientations with a single activation energy (dotted line) and a Gaussian distribution of energies (dashed line).

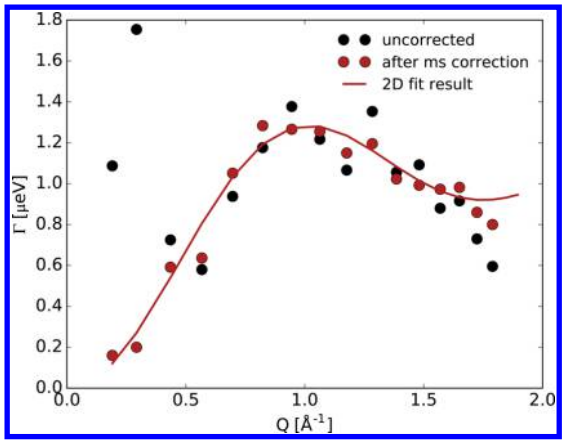

Figure 8. Quasielastic line widths of $Li[BH_4]_{1/3}[ND_2]_{2/3}$ as obtained from the model independent fit (black circles: raw data, red circles: after multiple scattering procedure) of the IN16B spectrum at $T = 360$ K and the result of the surface fit with eq 13 (red line).

Table 2. Parameters of the Best Fit IFWS Curves Obtained for the Uniaxial C_3-Rotation Model with a Gaussian Distribution of Activation Energies in the Temperature Range $T = 150-350$ K on IN16B

$Li[BH_4]_{1-x}[Y]_x$	Y	$\tilde{\tau}$, fs	E_A, kJ/mol	ΔE_A, kJ/mol
$x = 2/3$	NH_2	1.22(0.12)	25.2(0.2)	2.64(0.04)
$x = 2/3$	ND_2	2.57(0.18)	23.3(0.2)	2.59(0.04)
$x = 3/4$	NH_2	2.87(0.19)	24.3(0.2)	1.30(0.04)
$x = 3/4$	ND_2	1.62(0.11)	25.5(0.2)	1.66(0.05)

to the analogous approach for QENS spectra measured at a single temperature point.

There remains an open question about the nature of the dynamics that set in above 350 K in the borohydride rich samples ($x = 2/3$). The model-independent approach showed that the EISF of $Li[BH_4]_{1/3}[ND_2]_{2/3}$ did not depend on Q within the error margins and stayed at the level of 0.88 at $T = 360$ K and 0.82 at $T = 375$ K. This behavior excludes localized processes with the EISF tending to 1.0 at small Q-values. The possible explanation could be a diffusional process only for a certain fraction of particles in the system. This would corroborate the interpretation that the transition at 313 K is due to the melting of the side phase. To prove the conjecture, jump diffusion models have to be tested. The Chudley–Elliott model,[63] which considers jump vectors of constant length, l, and random direction, has the following Q-dependence of the quasielastic line width:

$$\Gamma(Q) = \frac{\hbar}{\tau_d}\left(1 - \frac{\sin(Ql)}{Ql}\right) \quad (13)$$

Here τ_d is the residence time. $\Gamma(Q)$ tends to 0 at small-Q values, however, the experimental line widths are severely distorted in this Q-range due to the multiple scattering (Figure 8). The iterative correction procedure involving eq 13 yields $l = 4.4 \pm 0.6$ Å and $\tau_d = 0.62 \pm 0.06$ ns at $T = 360$ K for approximately 12% of the $[BH_4]^-$ units, but the agreement between the experimental data and the Chudley–Elliot model at $T = 375$ K is significantly worse. This is an indication that eq 13 can serve only as a rough approximation and a more detailed study is required to clarify the motion mechanism in this temperature range.

CONCLUSIONS

In this work we obtained a coherent picture of anion reorientaional dynamics in the lithium amide-borohydrides $Li[BH_4]_{1-x}[NH_2]_x$ ($2/3 \leqslant x \leqslant 3/4$) by means of QENS. The experiments have been carried out on two different time scales (~1 ns on IN16B and ~1 ps on FOCUS) and in the temperature range of 5–425 K. Deuterium labeling has clearly demonstrated that the quasielastic signal in the studied time and temperature range originates mainly from the $[BH_4]^-$ units, whereas the $[NH_2]^-$ reorientational dynamics appeared to be too slow to be resolved. To describe motions of the $[BH_4]^-$ tetrahedra, we have developed a detailed model supported by the MD simulations and based on C_3-reorientations with different jump rates for an extended temperature range. The proposed model was validated by the results for the well studied bulk $LiBH_4$ and allowed us to identify three processes in the lithium amide-borohydrides, which can be resolved in successive order as the temperature increases.

The fastest process with the activation energy of 3.6 kJ/mol was detected on FOCUS in the temperature range of 250–300 K. The geometry of this motion is connected with small amplitude jumps close to the equilibrium positions. We tentatively ascribe this process to the $[BH_4]^-$ tetrahedra. The second process is associated with the uniaxial C_3 reorientation of the borohydride units. It determines the shape of the IFWS/EFWS measured in the temperature range 130–350 K on IN16B and is one of the main contributions resolved at higher temperatures on FOCUS. Predominant C_3 reorientations were proved by our MD simulations and IR spectra. Finally, as temperature increases, the third relaxation component sets in, when the $[BH_4]^-$ tetrahedra start rotating around all four C_3 axes. The temperature dependence of both the second and the third component of the best conducting sample ($Li[BH_4]_{1/3}[NH_2]_{2/3}$, $x = 2/3$) exhibits a pronounced change in the activation energy above the phase transition at 313 K, consistent with the ionic conductivity measurement.[8] The analysis of the IFWS in an extended temperature range has shown that the same sample also features a broader distribution of activation energies as compared to the reference sample with $x = 3/4$. Moreover, there is a clear onset of presumably diffusional motion of $[BH_4]^-$ in the high-temperature range. Thus, enhanced anion dynamics and rotational disorder are closely related to the high Li-conductivity realized in BH_4-rich $Li[BH_4]_{1-x}[NH_2]_x$ compounds.

DOI: 10.1021/acs.jpcc.7b05651
J. Phys. Chem. C 2017, 121, 17693–17702

Our analysis approach is not limited to lithium amide-borohydrides and can be extended to a family of related compounds with reorientational processes on different time scales. We have demonstrated that sophisticated information on the geometry, relaxation times, and origin of dynamics can be reliably extracted from QENS spectra of multicomponent systems.

■ ASSOCIATED CONTENT

Supporting Information

The Supporting Information is available free of charge on the ACS Publications website at DOI: 10.1021/acs.jpcc.7b05651.

Jump models for reorientational dynamics of borohydride tetrahedra, time evolution of the spherical coordinates of hydrogen atoms in $[BH_4]^-$ and $[NH_2]^-$ as obtained from the MD calculations, and IR spectra in the wavenumber range 1000−1400 cm^{-1} (PDF)

■ AUTHOR INFORMATION

Corresponding Authors

*(A.R.) E-mail: Arndt.Remhof@empa.ch.
*(J.P.E.) E-mail: jan.embs@psi.ch.

ORCID

Hans Hagemann: 0000-0002-7183-8543
Jan P. Embs: 0000-0002-2816-2875

Notes

The authors declare no competing financial interest.

■ ACKNOWLEDGMENTS

Financial support by the Swiss National Science Foundation by the Sinergia project "Novel ionic conductors" under Contract Number CRSII2_160749/1 is gratefully acknowledged. The authors thank the Institute Laue−Langevin (ILL) for beam time on the IN16B backscattering spectrometer and the Swiss spallation neutron source SINQ, Paul Scherrer Institute for beam time on FOCUS. CPU allocation at PL-Grid is kindly acknowledged.

■ REFERENCES

(1) Pinkerton, F. E.; Meisner, G. P.; Meyer, M. S.; Balogh, M. P.; Kundrat, M. D. Hydrogen Desorption Exceeding Ten Weight Percent from the New Quaternary Hydride $Li_3BN_2H_8$. *J. Phys. Chem. B* **2005**, *109*, 6−8.

(2) Meisner, G. P.; Scullin, M. L.; Balogh, M. P.; Pinkerton, F. E.; Meyer, M. S. Hydrogen Release from Mixtures of Lithium Borohydride and Lithium Amide: A Phase Diagram Study. *J. Phys. Chem. B* **2006**, *110*, 4186−4192.

(3) Lai, Q.; Paskevicius, M.; Sheppard, D. A.; Buckley, C. E.; Thornton, A. W.; Hill, M. R.; Gu, Q.; Mao, J.; Huang, Z.; Liu, H. K.; et al. Hydrogen Storage Materials for Mobile and Stationary Applications: Current State of the Art. *ChemSusChem* **2015**, *8*, 2789−2825.

(4) Wolczyk, A.; Pinatel, E. R.; Chierotti, M. R.; Nervi, C.; Gobetto, R.; Baricco, M. Solid-state NMR and Thermodynamic Investigations on $LiBH_4$−$LiNH_2$ System. *Int. J. Hydrogen Energy* **2016**, *41*, 14475−14483.

(5) Matsuo, M.; Remhof, A.; Martelli, P.; Caputo, R.; Ernst, M.; Miura, Y.; Sato, T.; Oguchi, H.; Maekawa, H.; Takamura, H.; et al. Complex Hydrides with $(BH_4)^-$ and $(NH_2)^-$ Anions as New Lithium Fast-Ion Conductors. *J. Am. Chem. Soc.* **2009**, *131*, 16389−16391.

(6) Matsuo, M.; Orimo, S.-i. Lithium Fast-Ionic Conduction in Complex Hydrides: Review and Prospects. *Adv. Energy Mater.* **2011**, *1*, 161−172.

(7) Unemoto, A.; Matsuo, M.; Orimo, S.-i. Complex Hydrides for Electrochemical Energy Storage. *Adv. Funct. Mater.* **2014**, *24*, 2267−2279.

(8) Yan, Y.; Kühnel, R.-S.; Remhof, A.; Duchêne, L.; Reyes, E. C.; Rentsch, D.; Łodziana, Z.; Battaglia, C. A Lithium Amide-Borohydride Solid-State Electrolyte with Lithium-Ion Conductivities Comparable to Liquid Electrolytes. *Adv. Energy Mater.* **2017**, 1700294.

(9) Braga, M. H.; Murchison, A. J.; Ferreira, J. A.; Singh, P.; Goodenough, J. B. Glass-Amorphous Alkali-Ion Solid Electrolytes and their Performance in Symmetrical Cells. *Energy Environ. Sci.* **2016**, *9*, 948−954.

(10) Seino, Y.; Ota, T.; Takada, K.; Hayashi, A.; Tatsumisago, M. A Sulphide Lithium Super Ion Conductor is Superior to Liquid Ion Conductors for Use in Rechargeable Batteries. *Energy Environ. Sci.* **2014**, *7*, 627−631.

(11) Kamaya, N.; Homma, K.; Yamakawa, Y.; Hirayama, M.; Kanno, R.; Yonemura, M.; Kamiyama, T.; Kato, Y.; Hama, S.; Kawamoto, K.; et al. A Lithium Superionic Conductor. *Nat. Mater.* **2011**, *10*, 682−686.

(12) Sadikin, Y.; Brighi, M.; Schouwink, P.; Černý, R. Superionic Conduction of Sodium and Lithium in Anion-Mixed Hydroborates $Na_3BH_4B_{12}H_{12}$ and $(Li_{0.7}Na_{0.3})_3BH_4B_{12}H_{12}$. *Adv. Energy Mater.* **2015**, *5*, 1501016.

(13) Filinchuk, Y. E.; Yvon, K.; Meisner, G. P.; Pinkerton, F. E.; Balogh, M. P. On the Composition and Crystal Structure of the New Quaternary Hydride Phase $Li_4BN_3H_{10}$. *Inorg. Chem.* **2006**, *45*, 1433−1435.

(14) Chater, P. A.; David, W. I. F.; Anderson, P. A. Synthesis and Structure of the New Complex Hydride $Li_2BH_4NH_2$. *Chem. Commun.* **2007**, 4770−4772.

(15) Wu, H.; Zhou, W.; Udovic, T. J.; Rush, J. J.; Yildirim, T. Structures and Crystal Chemistry of Li_2BNH_6 and $Li_4BN_3H_{10}$. *Chem. Mater.* **2008**, *20*, 1245−1247.

(16) Singer, J. P.; Meyer, M. S.; Speer, R. M.; Fischer, J. E.; Pinkerton, F. E. Determination of the Phase Behavior of $(LiNH2)_c(LiBH4)_{1-c}$ Quaternary Hydrides through in Situ X-ray Diffraction. *J. Phys. Chem. C* **2009**, *113*, 18927−18934.

(17) Soulié, J.-P.; Renaudin, G.; Černý, R.; Yvon, K. Lithium Boro-Hydride $LiBH_4$: I. Crystal Structure. *J. Alloys Compd.* **2002**, *346*, 200−205.

(18) Hartman, M. R.; Rush, J. J.; Udovic, T. J., Jr.; Bowman, R. C.; Hwang, S.-J. Structure and Vibrational Dynamics of Isotopically Labeled Lithium Borohydride Using Neutron Diffraction and Spectroscopy. *J. Solid State Chem.* **2007**, *180*, 1298−1305.

(19) Remhof, A.; Łodziana, Z.; Martelli, P.; Friedrichs, O.; Züttel, A.; Skripov, A. V.; Embs, J. P.; Strässle, T. Rotational Motion of BH_4 Units in MBH_4 (M=Li, Na, K) from Quasielastic Neutron Scattering and Density Functional Calculations. *Phys. Rev. B: Condens. Matter Mater. Phys.* **2010**, *81*, 214304.

(20) Verdal, N.; Udovic, T. J.; Rush, J. J. The Nature of BH_4^- Reorientations in Hexagonal $LiBH_4$. *J. Phys. Chem. C* **2012**, *116*, 1614−1618.

(21) Martelli, P.; Remhof, A.; Borgschulte, A.; Ackermann, R.; Strässle, T.; Embs, J. P.; Ernst, M.; Matsuo, M.; Orimo, S.-I.; Züttel, A. Rotational Motion in $LiBH_4$/LiI Solid Solutions. *J. Phys. Chem. A* **2011**, *115*, 5329−5334.

(22) Verdal, N.; Udovic, T. J.; Rush, J. J.; Wu, H.; Skripov, A. V. Evolution of the Reorientational Motions of the Tetrahydroborate Anions in Hexagonal $LiBH_4$-LiI Solid Solution by High-Q Quasielastic Neutron Scattering. *J. Phys. Chem. C* **2013**, *117*, 12010−12018.

(23) Remhof, A.; Yan, Y.; Embs, J. P.; Sakai, V. G.; Nale, A.; de Jongh, P.; Łodziana, Z.; Züttel, A. Rotational Disorder in Lithium Borohydride. *EPJ Web Conf.* **2015**, *83*, 02014.

(24) Remhof, A.; Mauron, P.; Züttel, A.; Embs, J. P.; Łodziana, Z.; Ramirez-Cuesta, A. J.; Ngene, P.; de Jongh, P. Hydrogen Dynamics in Nanoconfined Lithiumborohydride. *J. Phys. Chem. C* **2013**, *117*, 3789−3798.

(25) Verdal, N.; Udovic, T. J.; Rush, J. J.; Liu, X.; Majzoub, E. H.; Vajo, J. J.; Gross, A. F. Dynamical Perturbations of Tetrahydroborate Anions in $LiBH_4$ due to Nanoconfinement in Controlled-Pore Carbon Scaffolds. *J. Phys. Chem. C* **2013**, *117*, 17983−17995.

(26) Lundén, A. On the Paddle-Wheel Mechanism for Cation Conduction in Lithium Sulphate. *Z. Naturforsch., A: Phys. Sci.* **1995**, *50*, 1067−1076.

DOI: 10.1021/acs.jpcc.7b05651
J. Phys. Chem. C 2017, 121, 17693−17702

(27) Hull, S. Superionics: Crystal Structures and Conduction Processes. *Rep. Prog. Phys.* **2004**, *67*, 1233.
(28) Soloninin, A. V.; Babanova, O. A.; Medvedev, E. Y.; Skripov, A. V.; Matsuo, M.; Orimo, S.-i. Nuclear Magnetic Resonance Study of Atomic Motion in the Mixed Borohydride-Amide $Na_2(BH_4)(NH_2)$. *J. Phys. Chem. C* **2014**, *118*, 14805−14812.
(29) Bée, M. *Quasielastic Neutron Scattering, Principles and Applications in Solid State Chemistry, Biology and Materials Science*; Adam Hilger: Bristol, U.K., 1988.
(30) Remhof, A.; Züttel, A.; Ramirez-Cuesta, T. A.; García-Sakai, V.; Frick, B. Hydrogen Dynamics in the Low Temperature Phase of $LiBH_4$ Probed by Quasielastic Neutron Scattering. *Chem. Phys.* **2013**, *427*, 18−21.
(31) Schouwink, P.; Hagemann, H.; Embs, J. P.; D'Anna, V.; Černý, R. Di-Hydrogen Contact Induced Lattice Instabilities and Structural Dynamics in Complex Hydride Perovskites. *J. Phys.: Condens. Matter* **2015**, *27*, 265403.
(32) Verdal, N.; Udovic, T. J.; Stavila, V.; Tang, W. S.; Rush, J. J.; Skripov, A. V. Anion Reorientations in the Superionic Conducting Phase of $Na_2B_{12}H_{12}$. *J. Phys. Chem. C* **2014**, *118*, 17483−17489.
(33) Verdal, N.; Udovic, T. J.; Rush, J. J.; Skripov, A. V. Quasielastic Neutron Scattering Study of Tetrahydroborate Anion Dynamical Perturbations in Sodium Borohydride due to Partial Halide Anion Substitution. *J. Alloys Compd.* **2015**, *645*, S513−S517.
(34) Skripov, A. V.; Soloninin, A. V.; Filinchuk, Y.; Chernyshov, D. Nuclear Magnetic Resonance Study of the Rotational Motion and the Phase Transition in $LiBH_4$. *J. Phys. Chem. C* **2008**, *112*, 18701−18705.
(35) Skoryunov, R.; Babanova, O.; Soloninin, A.; Skripov, A.; Verdal, N.; Udovic, T. Effects of Partial Halide Anion Substitution on Reorientational Motion in $NaBH_4$: A Nuclear Magnetic Resonance Study. *J. Alloys Compd.* **2015**, *636*, 293−297.
(36) Nosé, S. A Unified Formulation of the Constant Temperature Molecular Dynamics Methods. *J. Chem. Phys.* **1984**, *81*, 511−519.
(37) Kresse, G.; Furthmüller, J. Efficient Iterative Schemes for ab Initio Total-Energy Calculations Using a Plane-Wave Basis Set. *Phys. Rev. B: Condens. Matter Mater. Phys.* **1996**, *54*, 11169−11186.
(38) Kresse, G.; Joubert, D. From Ultrasoft Pseudopotentials to the Projector Augmented-Wave Method. *Phys. Rev. B: Condens. Matter Mater. Phys.* **1999**, *59*, 1758−1775.
(39) Perdew, J. P.; Burke, K.; Ernzerhof, M. Generalized Gradient Approximation Made Simple. *Phys. Rev. Lett.* **1996**, *77*, 3865−3868.
(40) Chater, P. A.; David, W. I. F.; Johnson, S. R.; Edwards, P. P.; Anderson, P. A. Synthesis and Crystal Structure of $Li_4BH_4(NH_2)_3$. *Chem. Commun.* **2006**, 2439−2441.
(41) FOCUS: Time-of-Flight Spectrometer. 2017; http://www.psi.ch/sinq/focus/.
(42) Mesot, J.; Janssen, S.; Holitzner, L.; Hempelmann, R. FOCUS: Project of a Space and Time Focussing Time-of-Flight Spectrometer for Cold Neutrons at the Spallation Source SINQ of the Paul Scherrer Institute. *J. Neutron Res.* **1996**, *3*, 293−310.
(43) IN16B, a Sub-Micro-eV Energy Resolution Backscattering Spectrometer with a very High Count Rate and Wide Dynamic Range. 2017; http://www.ill.eu/instruments-support/instruments-groups/instruments/in16b/characteristics/
(44) Remhof, A.; Burankova, T.; Duchêne, L.; Embs, J. P.; Frick, B.; Roedern, E. *Hydrogen Dynamics in Novel Solid-State Li Conductors*; Institut Laue-Langevin (ILL): DOI: 10.5291/ILL-DATA.7-03-150,2016.
(45) Frick, B.; Combet, J.; van Eijck, L. New Possibilities with Inelastic Fixed Window Scans and Linear Motor Doppler Drives on High Resolution Neutron Backscattering Spectrometers. *Nucl. Instrum. Methods Phys. Res., Sect. A* **2012**, *669*, 7−13.
(46) Richard, D.; Ferrand, M.; Kearley, G. J.; Bradley, A. D. The Lamp Book. 2013; http://www.ill.eu/?id/2024.
(47) Azuah, R. T.; Kneller, L. R.; Qiu, Y.; Tregenna-Piggott, P. L. W.; Brown, C. M.; Copley, J. R. D.; Dimeo, R. M. DAVE: A Comprehensive Software Suite for the Reduction, Visualization, and Analysis of Low Energy Neutron Spectroscopic Data. *J. Res. Natl. Inst. Stand. Technol.* **2009**, *114*, 341−358.
(48) Burankova, T. *Dynamics and Structure of Ionic Liquids by Means of Neutron Scattering*; Ph.D. Thesis; Saarland University: 2014.
(49) Müller, M.; Asmussen, B.; Press, W.; Senker, J.; Jacobs, H.; Büttner, H.; Schober, H. Orientational Order and Rotational Dynamics of the Amide Ions in Potassium Amide. II. Quasielastic Neutron Scattering. *J. Chem. Phys.* **1998**, *109*, 3559−3567.
(50) Blanchard, D.; Maronsson, J. B.; Riktor, M. D.; Kheres, J.; Sveinbjörnsson, D.; Gil Bardají, E.; Léon, A.; Juranyi, F.; Wuttke, J.; Lefmann, K.; et al. Hindered Rotational Energy Barriers of BH_4^- Tetrahedra in β-$Mg(BH_4)_2$ from Quasielastic Neutron Scattering and DFT Calculations. *J. Phys. Chem. C* **2012**, *116*, 2013−2023.
(51) Silvi, L.; Rohm, E.; Fichtner, M.; Petry, W.; Lohstroh, W. Hydrogen Dynamics in β-$Mg(BH_4)_2$ on the Picosecond Timescale. *Phys. Chem. Chem. Phys.* **2016**, *18*, 14323−14332.
(52) Buchter, F.; Łodziana, Z.; Mauron, P.; Remhof, A.; Friedrichs, O.; Borgschulte, A.; Züttel, A.; Sheptyakov, D.; Strässle, T.; Ramirez-Cuesta, A. J. Dynamical Properties and Temperature Induced Molecular Disordering of $LiBH_4$ and $LiBD_4$. *Phys. Rev. B: Condens. Matter Mater. Phys.* **2008**, *78*, 094302.
(53) Sköld, K. Effects of Molecular Reorientation in Solid Methane on the Quasielastic Scattering of Thermal Neutrons. *J. Chem. Phys.* **1968**, *49*, 2443−2445.
(54) Farrell, D. E.; Shin, D.; Wolverton, C. First-Principles Molecular Dynamics Study of the Structure and Dynamic Behavior of Liquid $Li_4BN_3H_{10}$. *Phys. Rev. B: Condens. Matter Mater. Phys.* **2009**, *80*, 224201.
(55) Farrell, D. E.; Wolverton, C. Structure and Diffusion in Liquid Complex Hydrides via ab Initio Molecular Dynamics. *Phys. Rev. B: Condens. Matter Mater. Phys.* **2012**, *86*, 174203.
(56) Michel, K. H. Incoherent Neutron Scattering and Molecular Reorientations in Crystals near Tc. *J. Chem. Phys.* **1973**, *58*, 1143−1146.
(57) Rush, J. J.; Graaf, L. A. d.; Livingston, R. C. Neutron Scattering Investigation of the Rotational Dynamics and Phase Transitions in Sodium and Cesium Hydrosulfides. *J. Chem. Phys.* **1973**, *58*, 3439−3448.
(58) D'Anna, V.; Lawson Daku, L. M. L.; Hagemann, H. Vibrational Spectra and Structure of Borohydrides. *J. Alloys Compd.* **2013**, *580*, S122−S124.
(59) D'Anna, V.; Lawson Daku, L. M. L.; Hagemann, H. Quantitative Spectra-Structure Relations for Borohydrides. *J. Phys. Chem. C* **2015**, *119*, 21868−21874.
(60) Soloninin, A. V.; Dimitrievska, M.; Skoryunov, R. V.; Babanova, O. A.; Skripov, A. V.; Tang, W. S.; Stavila, V.; Orimo, S.-i.; Udovic, T. J. Comparison of Anion Reorientational Dynamics in MCB_9H_{10} and $M_2B_{10}H_{10}$ (M = Li, Na) via Nuclear Magnetic Resonance and Quasielastic Neutron Scattering Studies. *J. Phys. Chem. C* **2017**, *121*, 1000−1012.
(61) Österberg, C.; Fahlquist, H.; Häussermann, U.; Brown, C. M.; Udovic, T. J.; Karlsson, M. Dynamics of Pyramidal SiH_3^- Ions in $ASiH_3$ (A = K and Rb) Investigated with Quasielastic Neutron Scattering. *J. Phys. Chem. C* **2016**, *120*, 6369−6376.
(62) Hagemann, H.; Filinchuk, Y.; Chernyshov, D.; van Beek, W. Lattice Anharmonicity and Structural Evolution of $LiBH_4$: an Insight from Raman and X-Ray Diffraction Experiments. *Phase Transitions* **2009**, *82*, 344−355.
(63) Egelstaff, P. A. *An Introduction to the Liquid State*; Academic Press: London and New York, 1967.

DOI: 10.1021/acs.jpcc.7b05651
J. Phys. Chem. C 2017, 121, 17693−17702